



**AFRL-RX-WP-TP-2012-0249**

**QUASIPERIODIC STRAIN BURSTS AND SELF-  
ORGANIZATION IN CRYSTAL MICROPLASTICITY  
(PREPRINT)**

**D.M. Dimiduk  
Metals Branch  
Metals, Ceramics & Nondestructive Evaluation Division**

**S. Papanikolaou, M.D. Uchic, and C.F. Woodward  
Yale University**

**W. Choi and J.P. Sethna  
Cornell University**

**S. Zapperi  
Consiglio Nazionale delle Ricerche and ISI Foundation**

**MARCH 2012**

**Approved for public release; distribution unlimited.**

*See additional restrictions described on inside pages*

**STINFO COPY**

**AIR FORCE RESEARCH LABORATORY  
MATERIALS AND MANUFACTURING DIRECTORATE  
WRIGHT-PATTERSON AIR FORCE BASE, OH 45433-7750  
AIR FORCE MATERIEL COMMAND  
UNITED STATES AIR FORCE**

## NOTICE AND SIGNATURE PAGE

Using Government drawings, specifications, or other data included in this document for any purpose other than Government procurement does not in any way obligate the U.S. Government. The fact that the Government formulated or supplied the drawings, specifications, or other data does not license the holder or any other person or corporation; or convey any rights or permission to manufacture, use, or sell any patented invention that may relate to them.

This report was cleared for public release by the USAF 88<sup>th</sup> Air Base Wing (88 ABW) Public Affairs Office and is available to the general public, including foreign nationals. Copies may be obtained from the Defense Technical Information Center (DTIC) (<http://www.dtic.mil>).

AFRL-RX-WP-TR-2012-0249 HAS BEEN REVIEWED AND IS APPROVED FOR PUBLICATION IN ACCORDANCE WITH ASSIGNED DISTRIBUTION STATEMENT.

//SIGNED//

//SIGNED//

---

ANDREW ROSENBERGER, Program Manager  
Metals Branch  
Metals, Ceramics & Nondestructive Evaluation Division

---

PAUL RET, Branch Chief  
Metals Branch  
Metals, Ceramics & Nondestructive Evaluation Division

//SIGNED//

---

CHARLES H. WARD, Division Chief  
Metals, Ceramics & Nondestructive Evaluation Division  
Materials and Manufacturing Directorate

This report is published in the interest of scientific and technical information exchange, and its publication does not constitute the Government's approval or disapproval of its ideas or findings.

\*Disseminated copies will show “//signature//” stamped or typed above the signature blocks.

<b>REPORT DOCUMENTATION PAGE</b>				<i>Form Approved</i> OMB No. 0704-0188	
<p>The public reporting burden for this collection of information is estimated to average 1 hour per response, including the time for reviewing instructions, searching existing data sources, gathering and maintaining the data needed, and completing and reviewing the collection of information. Send comments regarding this burden estimate or any other aspect of this collection of information, including suggestions for reducing this burden, to Department of Defense, Washington Headquarters Services, Directorate for Information Operations and Reports (0704-0188), 1215 Jefferson Davis Highway, Suite 1204, Arlington, VA 22202-4302. Respondents should be aware that notwithstanding any other provision of law, no person shall be subject to any penalty for failing to comply with a collection of information if it does not display a currently valid OMB control number. <b>PLEASE DO NOT RETURN YOUR FORM TO THE ABOVE ADDRESS.</b></p>					
<b>1. REPORT DATE (DD-MM-YY)</b> March 2012		<b>2. REPORT TYPE</b> Technical Paper		<b>3. DATES COVERED (From - To)</b> 1 March 2012 – 1 March 2012	
<b>4. TITLE AND SUBTITLE</b> QUASIPERIODIC STRAIN BURSTS AND SELF-ORGANIZATION IN CRYSTAL MICROPLASTICITY (PREPRINT)				<b>5a. CONTRACT NUMBER</b> In-house	
				<b>5b. GRANT NUMBER</b>	
				<b>5c. PROGRAM ELEMENT NUMBER</b> 62102F	
<b>6. AUTHOR(S)</b> D.M. Dimiduk (AFRL/RXLMD) S. Papanikolaou, M.D. Uchic, and C.F. Woodward (Yale University) W. Choi and J.P. Sethna (Cornell University) S. Zapperi (Consiglio Nazionale delle Ricerche and ISI Foundation)				<b>5d. PROJECT NUMBER</b> 4347	
				<b>5e. TASK NUMBER</b> 20	
				<b>5f. WORK UNIT NUMBER</b> LM121100	
<b>7. PERFORMING ORGANIZATION NAME(S) AND ADDRESS(ES)</b> Metals, Ceramics & Nondestructive Evaluation Division Metals Branch Air Force Research Laboratory, Materials and Manufacturing Directorate Wright-Patterson Air Force Base, OH 45433-7750 Air Force Materiel Command, United States Air Force				<b>8. PERFORMING ORGANIZATION REPORT NUMBER</b> AFRL-RX-WP-TP-2012-0249	
<b>9. SPONSORING/MONITORING AGENCY NAME(S) AND ADDRESS(ES)</b> Air Force Research Laboratory Materials and Manufacturing Directorate Wright-Patterson Air Force Base, OH 45433-7750 Air Force Materiel Command United States Air Force				<b>10. SPONSORING/MONITORING AGENCY ACRONYM(S)</b> AFRL/RXLM	
				<b>11. SPONSORING/MONITORING AGENCY REPORT NUMBER(S)</b> AFRL-RX-WP-TP-2012-0249	
<b>12. DISTRIBUTION/AVAILABILITY STATEMENT</b> Approved for public release; distribution unlimited.					
<b>13. SUPPLEMENTARY NOTES</b> The U.S. Government is joint author of this work and has the right to use, modify, reproduce, release, perform, display, or disclose the work. PA Case Number and clearance date: 88ABW-2012-0771, 14 Feb 2012. Preprint journal article to be submitted to Science Magazine. This document contains color.					
<b>14. ABSTRACT</b> When external stresses in a system – physical, social or virtual – are relieved through impulsive events, it is natural to focus on the attributes of separate avalanches. However, during the quiescent periods in between, stresses may be relieved through competing processes, such as slowly flowing water between earthquakes or thermally activated dislocation flow between plastic bursts. Such unassuming, smooth responses can have dramatic effects on the avalanche properties. Our thorough experimental investigation of slowly compressed Ni microcrystals, covering three orders of magnitude in nominal strain-rate, exhibits unconventional quasi-periodic avalanche bursts and higher critical exponents as the strain rate is decreased. Our analytic and computational study, naturally extending dislocation avalanche modeling to incorporate competing processes, reveals the emergence of avalanche oscillator scaling behavior, a novel critical state manifesting through self-organized oscillatory approaches toward a critical depinning point. We demonstrate that the predictions of our theory are consistently manifested in our experiments.					
<b>15. SUBJECT TERMS</b> avalanches, self-organization, crystal defects, dislocation dynamics, multifractal, plasticity of crystals					
<b>16. SECURITY CLASSIFICATION OF:</b>			<b>17. LIMITATION OF ABSTRACT:</b> SAR	<b>NUMBER OF PAGES</b> 40	<b>19a. NAME OF RESPONSIBLE PERSON (Monitor)</b> Andrew Rosenberger
<b>a. REPORT</b> Unclassified	<b>b. ABSTRACT</b> Unclassified	<b>c. THIS PAGE</b> Unclassified			<b>19b. TELEPHONE NUMBER (Include Area Code)</b> N/A

# Quasiperiodic strain bursts and self-organization in crystal microplasticity

S. Papanikolaou,<sup>1,2\*</sup> D. M. Dimiduk,<sup>3</sup> W. Choi<sup>4</sup>, J. P. Sethna<sup>4</sup>, M. D. Uchic<sup>2</sup>,  
C. F. Woodward<sup>2</sup>, S. Zapperi<sup>5,6</sup>

<sup>1</sup> Department of Mechanical Engineering and Materials Science, Yale University,  
New Haven, Connecticut, 06520-8286, USA

<sup>2</sup> Department of Physics, Yale University, New Haven, Connecticut, 06520-8120, USA

<sup>3</sup>Civ USAF AFMC AFRL/RXLMD

<sup>4</sup>LASSP, Department of Physics, Clark Hall, Cornell University, Ithaca, NY 14853-2501,

<sup>5</sup>CNR - Consiglio Nazionale delle Ricerche, IENI, Via R. Cozzi 53, 20125 Milano and

<sup>6</sup>ISI Foundation, Viale S. Severo 65, 10133 Torino, Italy

\*To whom correspondence should be addressed; E-mail: stefanos.papanikolaou@yale.edu.

**When external stresses in a system – physical, social or virtual – are relieved through impulsive events, it is natural to focus on the attributes of separate *avalanches*. However, during the quiescent periods in between, stresses may be relieved through competing processes, such as slowly flowing water between earthquakes or thermally activated dislocation flow between plastic bursts. Such unassuming, smooth responses can have dramatic effects on the avalanche properties. Our thorough experimental investigation of slowly compressed Ni microcrystals, covering three orders of magnitude in nominal strain-rate, exhibits unconventional *quasi*-periodic avalanche bursts and higher critical exponents as the strain rate is decreased. Our analytic and computational study, naturally extending dislocation avalanche modeling to incorporate competing processes, reveals the emer-**

**gence of *avalanche oscillator scaling* behavior, a novel critical state manifesting through self-organized oscillatory approaches toward a critical depinning point. We demonstrate that the predictions of our theory are consistently manifested in our experiments.**

Physical systems under slowly increasing stress may respond through abrupt events. Such jumps in observable quantities are abundant (1), from Barkhausen noise (2) to plastic flow (3–5) and earthquakes (6). Even though events appear randomly sized and placed, the statistical properties of avalanches are universal, defining well understood non-equilibrium universality classes: The main unifying concept is the *depinning* of an interface under an external field (1,7). An implicit assumption underlying these concepts is that all other coexisting physical processes are either *too fast* and thus average out, or *too slow* rendering a static approximation valid. However, the latter assumption is not always true if the slow processes rearrange the pinning landscape at rates comparable to the external field driving rates. For as the fast avalanches are scale invariant, the whole timeseries, including the waiting intervals between the fast events, is also scale invariant (8). It is there within the waiting intervals that a slow restructuring of the pinning field can thrive and alter universal predictions as observed by Jagla (9).

While intermittent plastic flow is well known (10), only recently was it shown as statistically akin to universal mean-field avalanche behavior in the quasistatic limit. Investigations of the phenomenon utilized a wide variety of techniques, including acoustic emission from deforming ice (3), high resolution extensometry of tensile strained Cu (11) and microcrystal compression tests for FCC and BCC crystals, including Ni (4), Al (12), Mo (13) and LiF (14). However, most of these studies covered only a narrow range of nominal high strain rates. Preliminary evidence that suggests a more complex physical picture, was discussed by some of us in Ref. (15), where a rate dependence of the cumulative strain event size distributions was observed. In our experiments, Ni microcrystals of comparatively large dimensions, having diameters between

18 and 30  $\mu\text{m}$ , were uniaxially compressed (15). By controlling the applied external stress to maintain a *nominal* strain rate and by detecting slip with extremely sensitive extensometry, we track the crystal displacements in time. In order to study the rate dependence, we perform our experiments at three different nominal strain rates ( $10^{-4}/\text{s}$ ,  $10^{-5}/\text{s}$ ,  $10^{-6}/\text{s}$ ). For each sample, the timeseries of the displacement time derivative is filtered using optimal Wiener filtering methods adapted for avalanche timeseries (16), and avalanche events are appropriately defined without using thresholding.

As plastic deformation proceeds in the micropillars, the dislocation ensemble evolves at different time scales. The most apparent activity is associated with fast glide processes which produce stochastic bursts of deformation. Concurrently and in between these events, other less observable processes (cf. Fig. 1) contribute to collective *slower relaxations*. Like glide, these too are *thermally activated processes* accessible at these high levels of stress, but having different activation barriers, for example: the viscoelastic response of the dislocation forests after fast avalanche strain bursts, the localized dislocation climb motion in directions other than the glide plane under high local stresses, and also the cross-slip processes of dislocations shifting between glide planes are slow processes compared to the avalanche events (17). They all compete to minimize the far field stress while changing the local stress landscape and bypassing the glide process. They affect dislocation slip, but at a slower rate than avalanche glide (18). In our experiments, we classify as “slow relaxation” all the deformation that does not belong to avalanches of the scaling regime. Using this definition, the slow relaxation fraction increases drastically at the two slowest strain rates. Thus, the rate dependence of the avalanche size distribution (Fig. 2(c)) occurs when the nominal strain-rate becomes comparable to the rate of the slow relaxation processes (cf. Fig. 1). Although the exact mechanisms are unknown, one localized reorganization mechanism possible at these large local stresses and low temperatures ( $0.17T_m$  ( $\sim 300\text{K}$ )) (18) could be tied to newly discovered unconventionally large cross-slip

rates, as calculated for similar conditions to our experiments (19). For our purposes, and regardless of the type of relaxation mechanisms, we focus on the experimental fact that relaxation and driving rates become comparable. We phenomenologically incorporate the slow relaxation into our model in a simple and intuitive manner and then *a posteriori* show that our results are independent of the particular form of relaxational dynamics (see SOM).

The time series of slip event sizes  $S$ , labelled by their beginning time, display a striking dependence on the driving rate. After we smooth the timeseries over a fixed window of 400s and then rescale the time axis to display comparable strain evolution, a very clear (cf. Fig. 2(a)) quasiperiodic behavior emerges at the  $10^{-6}/\text{s}$  nominal rate. The emergent time period is observed to display an exponential dependence on the nominal strain rate, while its magnitude reaches  $\sim 8$  hrs (for  $10^{-6}/\text{s}$ ), consistently much larger than the length we chose for the fixed window averaging (cf. Fig. 1(c)). This qualitative change in the behavior is also reflected within statistical distributions of  $S$ : The size distribution shows a power law behavior ( $P(S) \sim S^{-\tau}$ ) for all studied strain rates ( $10^{-4}/\text{s}$ ,  $10^{-5}/\text{s}$ ,  $10^{-6}/\text{s}$ ), but the value of the power law exponent drifts from  $\sim 1.5$  (consistent with Refs. (4, 20)) to a higher and unexpected value of  $\sim 2.0$  (cf. Fig. 2(c)). An analogous behavior is observed for the durations  $T$  of the avalanches and their correlation with the sizes (cf. SOM); although there are concerns about the accuracy of these durations, given the response time of the apparatus and the frequency of the data recorded (15).

Our explanation of the experimental data builds on the model framework of dislocations moving through a disordered landscape of forest dislocations, on a single slip plane under the application of shear stress. This is a successful picture for avalanches during stage I plasticity (20–23) that strongly relies on well-understood models of 2+1 dimensional interface depin-

ning (7). Our model represents a minimal generalization *via* an added relaxation term,  $D$ ,

$$\frac{d\phi(\mathbf{r})}{dt} = \overbrace{D \left( \frac{\sigma(\mathbf{r})}{\mu} \right)^n \Theta(\sigma(\mathbf{r}))}^{(I)} + \overbrace{\frac{1}{\mu\epsilon} (\sigma(\mathbf{r}) - \sigma_f(\mathbf{r})) \Theta(\sigma(\mathbf{r}) - \sigma_f(\mathbf{r}))}^{(II)} . \quad (1)$$

where  $\mu$  is the shear modulus of the system, and  $\epsilon \ll 1$ . Here,  $\phi$  denotes the basic slip variable of the system, which is the  $yx$ -component (Burgers vector along  $x$ ) of the plastic distortion tensor, considering only infinite dislocations along  $z$  on  $xz$  slip planes (23). Part (I) of Eq. 1 denotes the coarse-grained slow relaxation of edge dislocations, assuming a rate  $D$  at a fixed temperature. Only positive slip motion is considered to simplify our simulations (24). With  $D \sim \exp(-\Delta/T)$ , we define an effective rate of thermally activated processes ( $\Delta$  is an effective energy barrier to such processes) that lead to slow relaxation. For simplicity, we set the exponent  $n = 1$ , since our conclusions do not qualitatively depend upon it. The applied stress is the  $xy$ -component of the stress tensor,

$$\sigma(\mathbf{r}) = \sigma_{\text{ext}} + \sigma_{\text{int}}(\mathbf{r}) + \sigma_{\text{hard}}(\mathbf{r}) = Mct + \int d^2\mathbf{r}' K(\mathbf{r} - \mathbf{r}') \phi(\mathbf{r}') - k\phi(\mathbf{r}) . \quad (2)$$

We consider a stress-controlled test in a stationary plastic regime ( $\sigma_{\text{ext}} \equiv Mct$ ) (25), where  $M$  is a machine stiffness, so that  $c$  has strain-rate units. In this framework, the relative timescales of the relaxation and stress rate increase are controlled by the dimensionless parameter  $R \equiv D/c$ . Part (II) of Eq. 1 denotes the fast glide process which controls the avalanche dynamics. Hardening is phenomenologically represented via a coefficient  $k$  that controls the distance of the system from its non-equilibrium depinning critical point. For clarity, we separate the relevant timescales by considering  $\epsilon \ll 1$ , leading to infinitely fast avalanches compared to the slow relaxation process.  $\sigma_f$  denotes the uncorrelated local pinning potential, due to dislocation forests. Finally,  $\sigma_{\text{int}}$  is chosen to contain the appropriate interaction kernel  $K$  for single slip straight edge dislocations (23). However, our main qualitative conclusions are independent of the kernel, and thus are equally applicable to other models of avalanches in plasticity (26).

The model of Eqs. 1 and 2 is solved by explicit integration with an Euler step until the condition  $\sigma(\mathbf{r}) > \sigma_f(\mathbf{r})$  is satisfied for some point  $\mathbf{r}$ , at which point an avalanche is triggered. For no relaxation ( $D=0$ ), the avalanches display statistics consistent with the predictions of the mean-field theory of interface depinning (1,5). As the relaxation  $D$  increases, both the critical exponent  $\tau$  for strain jump sizes  $S$  ( $P(S) \sim S^{-\tau}$ ) and the critical exponent  $\alpha$  for event durations  $T$  ( $P(T) \sim T^{-\alpha}$ ), increase substantially (cf. Fig. 2(b), SOM). However, the dependence of  $\langle S \rangle$  on the duration  $T$  ( $\langle S \rangle \sim T^{1/\sigma\nu z}$ ) remains unaltered ( $1/\sigma\nu z \simeq 2$ ), signifying that the universality class of the underlying non-equilibrium critical point remains unaltered while some critical exponents increase. In the context of mean-field theory, remotely similar behavior takes place when the driving rate  $c$  is increased (16) leading to avalanche overlap, unrelated though to our results which hold when  $c \rightarrow 0$  keeping  $R$  fixed (and  $> 1$ ).

The increase of the exponents is accompanied by a *quasiperiodic* behavior, signified by large slip events (cf. Fig. 2(b)): If one considers the average avalanche size in a window (cf. Fig. 2(b)), similar to the experimental study but without strain from relaxation included, it is clear that the  $D = 0$  flat-in-time profile is replaced by strongly oscillating profiles in the presence of slow relaxation ( $D > 0$ ). The average avalanche size ( $D = 0$ ) is inversely related to the hardening coefficient  $k$ ,  $k \sim \langle S \rangle^{-\sigma_k}$  with  $\sigma_k \simeq 1$ . Thus, there is a distribution of hardening coefficients being effectively sampled, reflecting local heterogeneity. We assume that such a distribution  $g(k')$  biases the integration, over all possible hardenings  $k'$ , of the size probability distribution of the  $D = 0$  model, leading to the observed *dynamically integrated* size distribution. That is, a curve in Fig. 2(d) may be obtained as

$$P_{\text{int}}(S) = \int_0^\infty g(k')P(S, k')dk' , \quad (3)$$

For example, assuming that  $g(k') = \text{const.}$  for any  $k' < k_0$  and zero above a limiting  $k_0$ , then we simply have at  $D/c \gg 1$ ,  $P_{\text{int}}(S) = S^{-\tau-\sigma_k}\mathcal{P}(Sk_0^{1/\sigma_k})$ , yielding a higher effective sizes-

exponent  $\tilde{\tau} \equiv \tau + \sigma_k$  for slow strain rates, with  $\tilde{\tau} = 5/2$  at mean-field. However, typically,  $g(k')$  might have a more complicated functional form, allowing for a large range of possible  $\tilde{\tau}$ s.

The profound effects of slow rate processes within our dislocation model and the comparison with experiments forces us to ask: Are our findings general? To make analytical progress toward an answer consider the “susceptibility to jumping”  $\rho$ , defined as the number of degrees of freedom that slip after the trigger slip. On average in our model  $\langle \rho \rangle$  is proportional to the hardening coefficient ( $\langle \rho \rangle \propto 1 - k$ ). In traditional mean-field models of interface depinning ( $I$ ), this quantity describes the “distance” of the system from the critical point and is considered saturated to a fixed point value after short-time transients (steady state). When  $\rho \ll 1$ , the system is far from the critical point, while the system is near critical when  $\rho \simeq 1$ . Numerical solutions to Eq. 1 verify that the additional relaxation process affects  $\rho$  in an unusual way: When an avalanche with size  $S_t$  takes place,  $\rho$  instantaneously decreases in a way proportional to the magnitude of  $S_t$ , while it increases linearly when there are no avalanche events. In a minimal sense, we suggest that the basic physical mechanism behind the behavior of Eq. 1 (with  $c \rightarrow 0$  but  $R$  fixed) is given by the behavior of the susceptibility to jumping  $\rho$ , whose basic characteristics can be described by the following Markov process,

$$\rho_{t+1} - \rho_t \equiv \Delta\rho_t = c_d \left(1 - \frac{S_t}{\bar{S}}\right). \quad (4)$$

where  $S_t$  is picked from the mean-field size distribution  $P(S_t) = N S_t^{-3/2} e^{-S_t/S_0}$  (where  $N$  is a normalization factor and  $S_0 = a/(1 - \rho_t)$ ) ( $I$ ) and the step  $c_d$  shall be thought as being proportional to  $R$ . The well-known avalanche mean-field behavior is described by the trivial  $c_d \rightarrow 0$  fixed point (analogous to higher experimental strain rates). The size of the avalanche at time  $t$ ,  $S_t$ , is a stochastic variable which mimics the avalanche dynamics described by Eq. 1 (which is in the mean-field universality class). When  $c_d \ll 1$ ,  $\rho$  increases in small steps towards the fixed point given by  $\rho_0 = 1 - \frac{\pi a^2}{4S^2}$  with average size  $\bar{S} = \frac{a}{2} \sqrt{\pi/(1 - \rho_0)}$  ( $a$  being the minimum

accessible size) saturating at a value similar to that for the traditional depinning dynamics (cf. Fig. 3 left). However, there is a finite probability of a large (but *not* infinite!) avalanche which takes the system far from the fixed point, with  $\Delta\rho_t$  large and negative. If  $\delta S = S_t - \bar{S}$ , then  $\Delta\rho_t = -c_d\delta S/\bar{S} \sim -1$  indicates the emergence of a novel quasiperiodic behavior (cf. Fig.1(b)) showing large negative  $\rho$ -jumps with  $S_t$  being large *rare* avalanche events, much larger than  $\bar{S}$ . Now,  $\rho_0$  is not able to have the essential defining role as a steady-state susceptibility as for the traditional critical behavior, and  $\rho$  performs a *Sisyphean* task constantly ascending towards  $\rho_0$ . In this way, the distribution of  $\rho$  effectively flattens as  $c_d$  increases (low experimental strain rates) (cf. Fig. 3 right), leading to integrated exponents (cf. Eq. 3). In a consistent manner, the analogous distribution for the model in Eq. 1 flattens as  $R$  increases (cf. Fig. 3 right (inset)).

The rare  $\delta S$  events scale with  $S_0 \sim 4\bar{S}^2/(\pi a)$  and qualitatively, the transition between the two regimes takes place when  $c_d \sim a\pi/(4\bar{S}) \sim 1/(\bar{S}/a)$ . Numerically, we get a consistent “phase diagram” line (cf. Fig.3 lower) which separates the two qualitative behaviors. We shall mention that our model shares a strong resemblance to the case of relaxation limit cycle oscillations near a singular Hopf bifurcation with stochastic perturbations (27), a dynamical system similar to Sōzu, the traditional Japanese gardening device.

Contemporary observations have revealed novel and creative mechanical behaviors of crystals in the microscale. Together with the size effects (28, 29) and the emergence of avalanche slip events (3, 4), the importance of often neglected slow processes on intermittency has now come to light. Our study provides basic elements for constructing a much desired accurate multiscale theory of microscale plasticity (30). By incorporating the complex microscopic slow dynamics of dislocations operating between the fast glide processes, it is possible to capture the complete interplay between local stress concentrations that lead to violent bursts and the collective relaxational dynamics of the dislocation environment over longer times. These experiments

in the world of “small” and the associated theory that we developed, force us to reconsider our understanding of the world of “large”, earthquake faults (6), sheared amorphous solids (31) and other depinning processes, setting additional constraints. Whenever the mechanism that drives avalanche dynamics competes with other slow coexisting processes to lower stress, when the driving is slow enough, the nature of the avalanche dynamics is modified and gives rise to critical quasiperiodic bursts.

## References

1. D. S. Fisher, Collective transport in random media: from superconductors to earthquakes, *Phys. Reports* **301**, 113 (1998), and J. Sethna, K. Dahmen, C. Myers, Crackling noise, *Nature* **410**, 242 (2001).
2. G. Durin, S. Zapperi, The Barkhausen Effect, in *The Science of Hysteresis*, vol. II, G. Bertotti and I. Mayergoyz, (Elsevier, 2006).
3. M. C. Miguel, A. Vespignani, S. Zapperi, J. Weiss, J.-R. Grasso, Intermittent dislocation flow in viscoplastic deformation, *Nature* **410**, 667 (2001), and J. Weiss, F. Lahaie, J. Grasso, Statistical analysis of dislocation dynamics during viscoplastic deformation from acoustic emission, *J. Geophys. Res* **105**, 433 (2000).
4. D. M. Dimiduk, C. Woodward, R. LeSar, M. D. Uchic, Scale-Free Intermittent Flow in Crystal Plasticity, *Science* **312**, 1188 (2006).
5. M. Zaiser, Scale invariance in plastic flow of crystalline solids, *Adv. Phys.* **55**, 185 (2006).
6. Y. Ben-Zion, Collective Behavior of Earthquakes and Faults: Continuum-Discrete Transitions, Progressive Evolutionary Changes and Different Dynamic Regimes, *Rev. Geophysics*, **46**, RG4006, (2008).

7. M. Kardar, Nonequilibrium dynamics of interfaces and lines, *Physics Reports* **301**, 85 (1998).
8. P. Le Doussal, K. J. Wiese, Driven particle in a random landscape: Disorder correlator, avalanche distribution, and extreme value statistics of records, *Phys. Rev. E* **79**, 051105 (2009).
9. E. A. Jagla, Realistic spatial and temporal earthquake distributions in a modified Olami-Feder-Christensen model., *Phys. Rev. E* **81**, 046117 (2010), and E. A. Jagla, Towards a modeling of the time dependence of contact area between solid bodies, *J. Stat. Mech.* **2010**, P06006 (2010).
10. R. Becker, E. Orowan, Über sprunghafte Dehnung von Zinkkristallen, *Z. Phys.* **79**, 566 (1932).
11. J. Weiss, *et al.*, Evidence for universal intermittent crystal plasticity from acoustic emission and high-resolution extensometry experiments, *Physical Review B* **76**, 224110 (2007).
12. A. H. W. Ngan, Stochastic theory for jerky deformation in small crystal volumes with pre-existing dislocations, *Philos. Mag. Lett.* p. 87 (2008).
13. M. Zaiser, *et al.*, Strain bursts in plastically deforming Molybdenum micro- and nanopillars, *Philos. Mag.* **88**, 3861 (2008).
14. D. M. Dimiduk, E. M. Nadgorny, C. Woodward, M. D. Uchic, P. A. Shade, An experimental investigation of intermittent flow and strain burst scaling behavior in LiF crystals during microcompression testing, *Philos. Mag.* **90**, 3621 (2010).
15. D. M. Dimiduk, M. D. Uchic, S. I. Rao, C. Woodward, T. A. Parthasarathy, Overview of experiments on microcrystal plasticity in FCC-derivative materials: selected challenges for

- modelling and simulation of plasticity, *Modelling Simul. Mater. Sci. Eng.* **15**, 135 (2007).
16. S. Papanikolaou, *et al.*, Universality beyond power laws and the average avalanche shape, *Nat. Phys.* **7**, 316 (2011).
  17. The calculation of the actual speed of these processes during plasticity is a very complicated problem that we do not address here. But it is natural to expect that climb, cross-slip and viscoelastic response partially happen in a slower than glide manner.
  18. M. Kassner, M.-T. Perez-Prado, *Fundamentals of Creep in Metals and Alloys* (Elsevier, 2004).
  19. S. I. Rao, *et al.*, Activated states for cross-slip at screw dislocation intersections in face-centered cubic nickel and copper via atomistic simulation, *Acta Mater.* **58**, 5547 (2010).
  20. F. F. Csikor, C. Motz, D. Weygand, M. Zaiser, S. Zapperi, Dislocation Avalanches, Strain Bursts, and the Problem of Plastic Forming at the Micrometer Scale, *Science* **318**, 251 (2007).
  21. M. Koslowski, R. LeSar, R. Thomson, Avalanches and scaling in plastic deformation, *Phys. Rev. Lett.* **93**, 125502 (2004).
  22. S. Yefimov, I. Groma, E. van der Giessen, A comparison of a statistical-mechanics based plasticity model with discrete dislocation plasticity calculations, *Journal of the Mechanics and Physics of Solids* **52**, 279 (2004).
  23. M. Zaiser, P. Moretti, Fluctuation phenomena in crystal plasticity—a continuum model, *J. Stat. Mech.* **8**, P08004 (2005).
  24. A. A. Middleton, Asymptotic uniqueness of the sliding state for charge-density waves, *Phys. Rev. Lett.* **68**, 670 (1992).

25. M. Zaiser, N. Nikitas, Slip avalanches in crystal plasticity: scaling of the avalanche cut-off, *Journal of Statistical Mechanics: Theory and Experiment* **2007**, P04013 (2007).
26. In the model by Koslowski *et al.* (21) where mixed dislocations are included, one would modify our definitions by considering a single  $xy$  slip plane, assume  $\phi$  to be the  $xy$  tensor component, and only apply the  $zx$  component of the stress.
27. C. Muratov, E. Vanden-Eijnden, Noise-induced mixed-mode oscillations in a relaxation oscillator near the onset of a limit cycle, *Chaos* **18**, 5111 (2008).
28. M. D. Uchic, D. M. Dimiduk, J. N. Florando, W. D. Nix, Sample Dimensions Influence Strength and Crystal Plasticity, *Science* **305**, 986 (2004).
29. J. R. Greer, W. C. Oliver, W. D. Nix, Size dependence of mechanical properties of gold at the micron scale in the absence of strain gradients, *Acta Materialia* **53**, 1821 (2005).
30. B. Devincre, T. Hoc, L. Kubin, Dislocation Mean Free Paths and Strain Hardening of Crystals, *Science* **320**, 1745 (2008).
31. C. E. Maloney, M. O. Robbins, Evolution of displacements and strains in sheared amorphous solids, *J. Phys: Cond. Mat.* **20**, 244128 (2008).
32. A. Corral, Point-occurrence self-similarity in crackling-noise systems and in other complex systems, *J. Stat. Mech.* p. P01022 (2009).
33. **Acknowledgements:** We would like to thank J. Guckenheimer, C. L. Henley, E. A. Jagla, E. Nadgorny, C. O' Hern, R. Thorne, D. Trinkle, E. van der Giessen and V. Vitelli for inspiring discussions. We acknowledge support from DOE-BES DE-FG02-07ER-46393 (SP, WC and JPS), the US AFOSR (DMD, CW and MU) and the ComplexityNet pilot project LOCAT (SZ).

**Figure 1 – Complexity of dislocation motion and slow relaxation during avalanche waiting intervals.** **Upper:** A schematic toy demonstration of the complex processes that dislocation experience. Lighter to darker color scale indicates time evolution. Under the application of stress, a dislocation loop nucleates and attempts to grow but it gets pinned on its slip plane (lighter color). Depinning to a larger loop configuration corresponds to a fast glide-slip burst, the most common dislocation slip. However, as the loop grows a screw dislocation segment undergoes *double cross-slip* to a parallel slip plane, in order to bypass the glide barriers. On the new plane, the dislocation loop glides and, ultimately it undergoes dislocation climb. **Lower Left:** A part of the timeseries of the plastic deformation of a Ni sample at  $10^{-6}$  rate. The avalanche phenomenon, when close to criticality, does not manifest itself only through the rather fast and violent scale-invariant bursts (16), but also through unavoidable long waiting times (8,32) where glide processes are inactive; It is due to this *scale-invariant* distribution of waiting times that slow, non-equilibrium stress minimizing processes can thrive, altering in a fundamental manner the properties of the critical avalanche behavior. **Lower Right:** The estimated percentage of strain accumulated in slow relaxation flow which does not amount to large, observable strain bursts is shown on the left (black): The percentage (relaxation strain/total final strain) strongly increases as the rate decreases. Experimental noise certainly contributes to the relaxation strain measured. On the right, a non-trivial *quasiperiod* (average period of intermittent oscillations) of organised avalanche behavior emerges and increases dramatically as the nominal rate decreases.

**Figure 2 – Experiments vs. Theory.** (a) Average avalanche size as a function of time for different strain rates. Avalanche sizes are averaged based on their start times in 400s windows. Note that the time axes are rescaled by the nominal strain rate, aligning the “strain scales”. For different, independently strained samples, clear *quasi*-periodic avalanche behavior emerges

as the nominal strain rate decreases. The period, as soon as it becomes apparent (0.4nm/s sample), stays of similar size in “strain scale” while it increases drastically in real time – a key prediction of the theory we present in this paper. (b) The stick-slip oscillations that are observed experimentally (a) are a typical characteristic of the explored model of Eq. 1. Here, we fixed the value of the relaxation rate and varied the actual strain-rate (by modifying  $c$ ), similarly to the situation in the experiments. We should mention that there is an overall scale that is freely modified in order to match the experiments. This gives us a unit of strain being  $2 \times 10^{-6}$  and a fast timescale unit of  $0.5s$ . We shall notice that there is a difference of the simulations’ timeseries from the experimental in (a) in that the detected events are the *actual* avalanche events without the distortion that would appear due to the strain coming from the slow relaxation. Ideally, this plot should experimentally emerge if the creep strain is removed. This difference is behind the overall scale difference of the two plots. (c) Rate dependence of the critical exponent of the probability distribution for the sizes of the displacement jumps. Even though the hardening coefficient for the different samples used is roughly similar ( $\pm 10\%$ ), the slope of the distribution increases as the nominal strain rate decreases. We shall notice that as the rate decreases a large collection of small, almost invisible events appear with similar probability in the distribution (not shown). (d) Similarly as in (c), the decrease of  $c$  leads to a “rate dependence” of the size distribution exponent (and other related exponents), which we explain in the text. The exponent drifts from the known  $\sim 1.5$ , reported also in the original Ref. (23), to approximately  $\sim 2.5$ , the limiting value for a “flat” distribution of  $\rho$ ’s (cf. Fig. 3). As we show in the Supplementary Information, it is clear that the high  $S$  bump near the cutoff fades away and flattens as  $k$  increases, even though the exponent stays virtually unaltered.

**Figure 3 – Effective modeling of the jumping susceptibility. Upper Left:** A plot portraying the behavior of the reduced, analytical model Eq. 4. As the rate  $c_d$  is increased, large noise

causes  $\rho(t)$  to oscillate between  $\rho \sim 1$  and small  $\rho$ , causing larger exponents, according to the discussion in the main text. **Upper Right:** The probability distribution of  $\rho$  as calculated from the solutions of the effective model Eq. 4. The distribution becomes flat as  $c_d$  increases, with  $\rho$  being “sampled” with equal probability during an oscillation. In the inset, the probability distribution of  $\langle S \rangle_{50}$  is shown for the simulations of Eq. 1, calculated by considering the timeseries of the events, regarded as instantaneous, and then averaged with a running window of size 50. The simulations have the same parameters as in (a). The histogram, shown in the appropriate scale ( $1 - 1/\langle S \rangle^2 \equiv \rho$ ) becomes flat, while being sharply peaked for small  $R$ . **Center:** The phase diagram which distinguishes the novel regime where the fluctuations of  $\rho$  are large enough to cause quasiperiodic oscillations from the traditional regime where  $\rho$  fluctuates weakly around the fixed-point value  $\rho_0$ . The line signifies the instability to quasiperiodic behavior  $c_d \sim 1/\bar{S}$  as described in the text. The points label the locations where simulations of Eq. 4 were performed and then, the critical exponent  $\tilde{\tau}$  was calculated using Eq. 3 at the points, with a final Gaussian interpolation for the color background.

**Figure 1 – Complexity of dislocation motion and creep during avalanche waiting intervals**

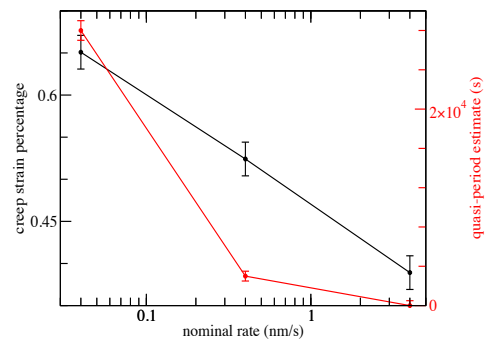
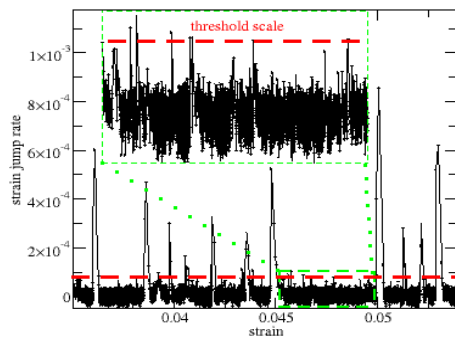
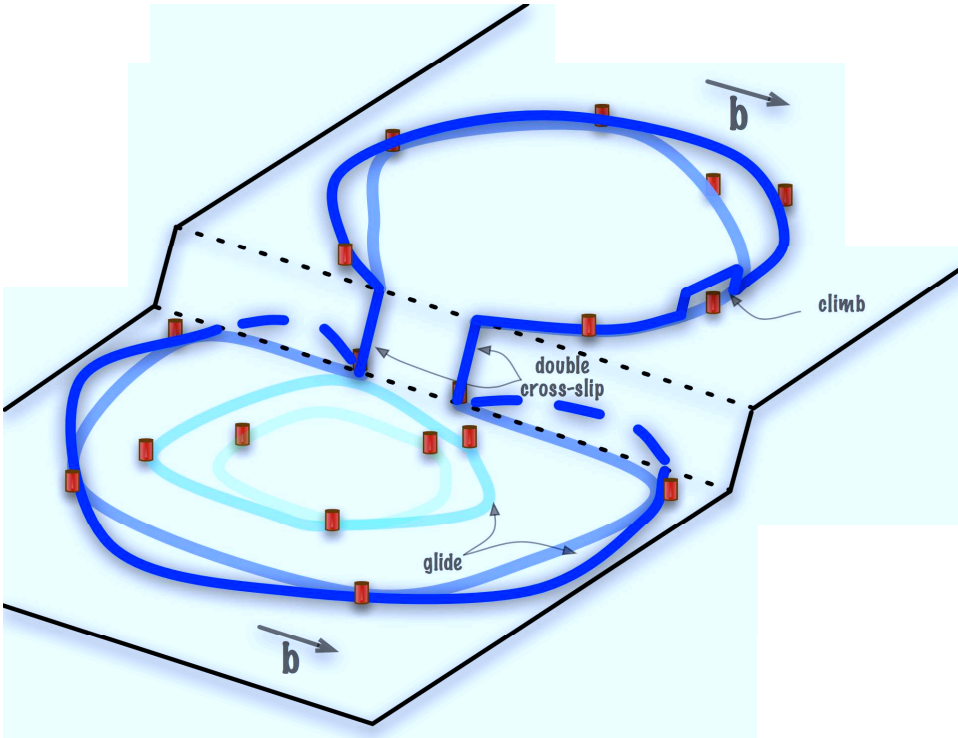


**Figure 2 – Experiments vs. Theory**

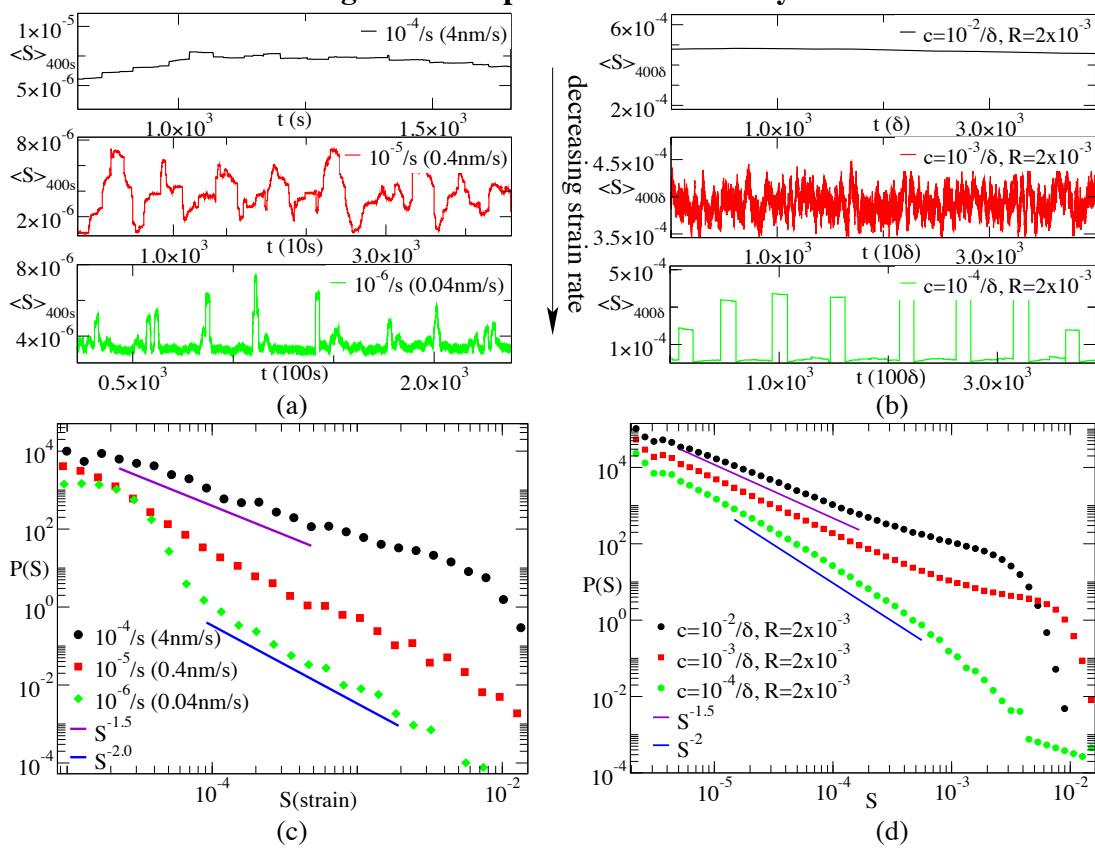
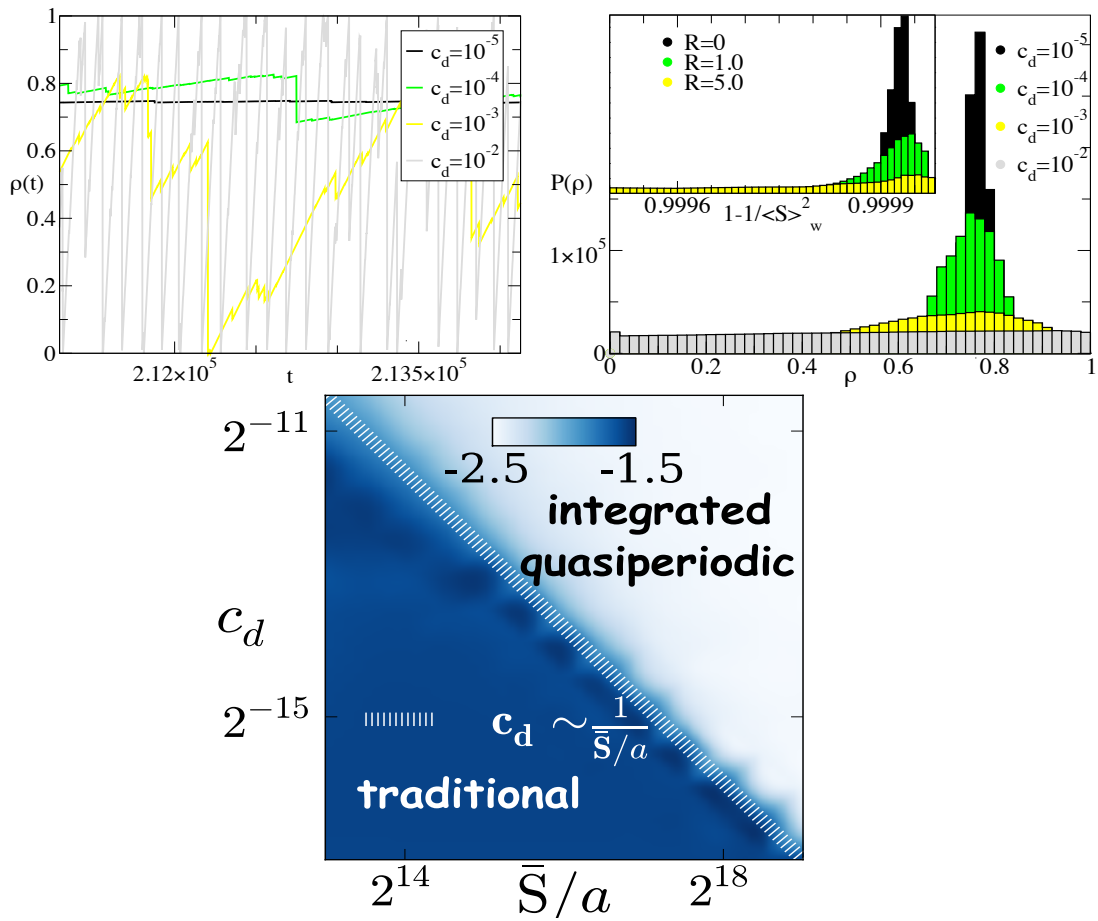


**Figure 3 – Effective modeling of the jumping susceptibility**



# Supporting Online Material for

## Quasiperiodic strain bursts and self-organization in crystal microplasticity

S. Papanikolaou,<sup>1,2\*</sup> D. M. Dimiduk,<sup>3</sup> W. Choi<sup>4</sup>, J. P. Sethna<sup>4</sup>, M. D. Uchic<sup>2</sup>,  
C. F. Woodward<sup>2</sup>, S. Zapperi<sup>5,6</sup>

<sup>1</sup> Department of Mechanical Engineering and Materials Science, Yale University,  
New Haven, Connecticut, 06520-8286, USA

<sup>2</sup> Department of Physics, Yale University, New Haven, Connecticut, 06520-8120, USA

<sup>3</sup>Civ USAF AFMC AFRL/RXLMD

<sup>4</sup>LASSP, Department of Physics, Clark Hall, Cornell University, Ithaca, NY 14853-2501,

<sup>5</sup>CNR - Consiglio Nazionale delle Ricerche, IENI, Via R. Cozzi 53, 20125 Milano and

<sup>6</sup>ISI Foundation, Viale S. Severo 65, 10133 Torino, Italy

\*To whom correspondence should be addressed; E-mail: stefanos.papanikolaou@yale.edu.

### This PDF file includes:

(A) Materials and Methods

(B) SOM Text

(C) Figs. S1 to S12

### (A) Materials and Methods

**Experimental:** The experimental measurements were performed using the methodology described in (10). The data are taken at time resolutions 5, 50 and 500 Hz for different samples, depending on the case. The nominal strain rates were  $10^{-4,-5,-6}$ /s with corresponding average platen velocities of 4, 0.4 and 0.04 nm/s, given the dimensions of the pillars. The experi-

mental timeseries were filtered using optimal Wiener filtering methods optimized for studying avalanches, as described in (3). Optimal Wiener filtering corresponds to a low-pass filter that has significant effects only at short timescales which are plagued by apparatus problems. In a similar fashion, as in Ref. (3), we performed adequate tests in order to confirm that the power-laws and the long-time quasiperiodic behavior are not related to the filtering procedure. The experimental data is available upon request.

**Theoretical:** In the simulations of Eq. 1, during diffusion, Euler time stepping is used to evolve the differential equation on a  $L \times L$  grid. During an avalanche, given that  $\epsilon \rightarrow 0$ , the stress is not increased and the relaxation term (I) does not participate in the evolution. This approximation was performed for clarity purposes, with qualitatively similar results with the case  $\epsilon = 1$ . In that case, the effect of diffusion is more visible and avalanches dissipate (for large  $D$ ) much smaller stress percentage, since the relaxation term dominates the behavior. During the avalanche process, we evolve the system by using cellular automata rules: when the total local stress crosses its  $\sigma_f$  threshold, the associated local slip  $\phi$  increases randomly with a normal distribution with mean 1 and variance 1. In the stress of Eq. 1, we have also added a term for regularizing purposes that slightly smoothens the slip profiles. It takes the form  $\alpha \nabla^2 \phi$  with very small  $\alpha = 0.05$ . We have checked for several system sizes (up to  $64^2$ ) that this term does not affect our reported results in any visible manner. Also, we note that this term is physically motivated, in as much as it is connected to the coarse-grained form of the stress generated by dislocation pile-ups (23). In our simulations we used a flat distribution ranged in  $(0, 1]$  for the quenched disorder  $\sigma_f(\mathbf{r})$ , following a typical protocol (1). The kernel  $K(\mathbf{r})$  has a continuum Fourier representation  $\tilde{K}(k) = -Ck_x^2k_y^2/(k_x^2 + k_y^2)^2$ (23), where we set  $C = 1$  for clarity purposes in our analysis. A modification of  $C$  modifies the strength of disorder required in the model in order to observe avalanche behavior, with no other changes. In all simulations using Eq. 1 (unless explicitly mentioned otherwise) the hardening coefficient  $k$  is selected from

the formula  $k = 2L^{0.85}/S_0$  where we chose  $S_0 = 1000$  with  $S_0$  being approximately equal to the cutoff size of the distribution that is derived for  $D = 0$ . The reason for this choice has to do with the fact that the nature of the kernel (23) is such that a fixed local hardening coefficient  $k$  does not set the cutoff for the size distribution. Rather, it allows for a weak increase with the system size. However, for our purpose (studies of  $D > 0$ ) it was crucial to have well controlled critical distributions for  $D = 0$ , independent of the system size, to identify the concrete effects of the relaxation on the distributions. In all plots we refer to the value of  $R = D/c$ .

In the simulations of Eq. 4, the stochastic equation was solved using random variables that follow the required power-law distribution with exponential cutoff, generated with the standard rejection method. During solving Eq. 4 numerically,  $\rho$  can jump above 1, a regime that we do not consider. There are several options to deal with the boundary condition at  $\rho = 1$  which are numerically very similar for large  $\bar{S}$  and small  $c_d$ . After a jump which takes  $\rho > 1$ , : i)  $\rho$  is reset to a random value between 0 and 1 (this method was used for the generation of Fig. 3 Center), ii)  $\rho$  is reset to a specific value (for example, 0), iii)  $\rho$  is set to be equal with the long-time average  $1 - 1/\bar{S}^2$ . We shall reiterate that these crossings ( $\rho > 1$ ) are finite-size effects and do not define the system's behavior at long times and in the limit of  $\bar{S} \rightarrow \infty$ , as we verified in both simulations of Eq. 1 (showing that the distribution “bump” consistently vanish with the system size) and Eq. 4 (showing that different treatments of the  $\rho = 1$  boundary lead to the same conclusion and phase boundary  $c_d \sim 1/\bar{S}$ ).

The codes used for the simulations of Eqs. 1 and 4 are written in Python and are available upon request.

## **(B) SOM Text**

In this supporting online material we

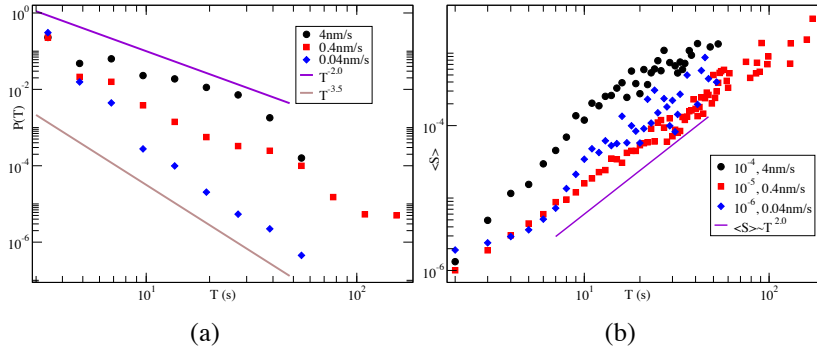


**Figure S1 – Duration Distributions and Average Size vs. Durations.** In association with the size distributions of Fig. 1(b), the duration distributions and average size for given duration plots, show a consistent behavior with theory (the prediction being  $\langle S \rangle \sim T^{1/\sigma\nu z}$  and at mean-field  $1/\sigma\nu z = 2$ ) (cf. Fig. S8). However, it is worth being sceptical about the importance of durations, given that they are very long compared to the expectations, given the magnitude of typical individual dislocation velocities (15, 19). Here, we just show that the whole behavior is roughly consistent with theoretical expectations, suggesting that the observed durations reflect, perhaps in a serendipitous manner, the theoretically expected behavior.

- (a) Show that the experimental results on the durations of the avalanches are consistent with the results expected from our theory, and present more details about the methodology for studying the rate dependent quasi-periodicity.
  - (b) Show that the simulations of Eq. 1 are consistent with the simple general model of Eq. 4 which explains the reported novel theoretical behavior.
  - (c) Explore analytically the properties of Eq. 4 and show that the crossover between the two found qualitative behaviors can be estimated quite accurately using the concept of the survival probability,
  - (d) Present more details from the simulations we performed using the model of Eq. 1, discuss results from other kernels and, present our conclusions on the generality of the effect.
- (a) Consistency of durations and more details on the experimental time-**

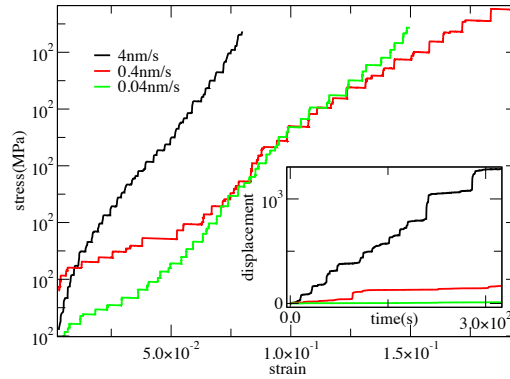


**Figure S2 – Stress vs. Strain and Strain vs. Time** (a) Selected stress - strain curves at different rates, displaying similar hardening coefficients and yield stresses. In the inset, the strain vs. time behavior is shown, vividly illustrating that the strain increases on average 10 and 100 times slower in the  $10^{-5}$  and  $10^{-6}$  tests.

## series

The study of avalanche durations in microplasticity has been scarce because the timescales observed (due to a very limited time resolution and apparatus' sensitivity) are many orders of magnitude larger (milliseconds) than the ones where the actual events are actually taking place (nanoseconds). Even though the observed events are believed to be well separated in time, avoiding avalanche overlaps, the internal avalanche temporal structure is questionable (2, 3, 4, 10, 15, 21). However, it is possible that the observed large events actually follow the statistics of the dislocation dynamics' critical behavior. Our study of the event durations and their clear relation to the event sizes suggest that this could be the case: In Figure S1(a), we see that the duration distribution displays a strong rate dependence with the associated critical exponent drifting from  $\sim 2$  to  $\sim 3$ , while the average size  $\langle S \rangle$  scales with the avalanche duration in a visibly similar manner, having an exponent  $\sim 2$ . ( $\langle S \rangle \sim T^2$ ) This behavior is consistent with our simulations, as discussed in (c) of this supplement. The critical exponent for durations  $\alpha$  drifts from 2 to  $2 + 1 = 3$ , while the relation between the average size to its duration remains invariant. In this sense, the results resemble the effect of a finite driving rate  $c$  (avalanche

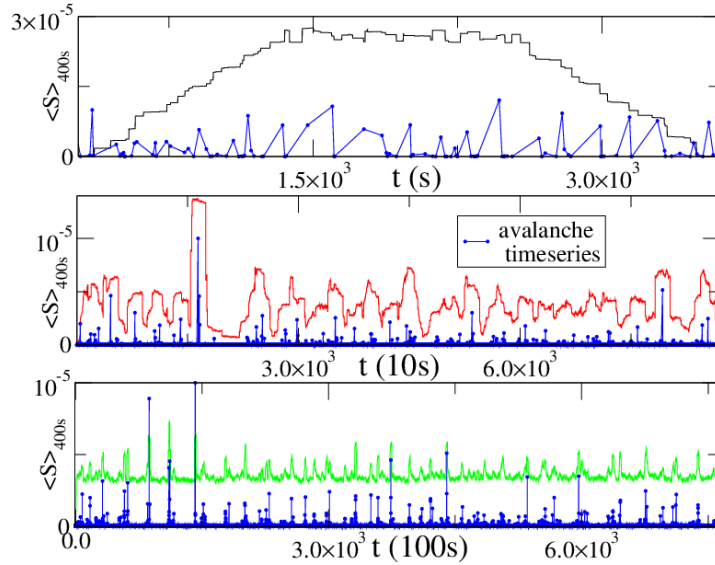


**Figure S3 – Windowed event timeseries.** Here, we display the full timeseries of Figure 1(c) for three selected samples studied, in order to show that the periodicity we identified is not an artifact but characterizes the whole deformation process. The actual event timeseries (blue color, before smoothening) is also present in order to show that the periods we identified are strongly correlated with strong peaks in the event sizes at the high points of the periods.

overlap) in the mean-field avalanche model (3), wherein the average size scales as  $T^{1/\sigma\nu z}$  and  $\sigma\nu z$  remains invariant when  $c$  is modified.

The phenomenological hardening coefficient used in the simulations of Eq. 1 is held fixed without assuming any time or rate dependence. However, experimentally, we observe a weak but visibly complicated rate dependence of the hardening coefficient. The stress vs. strain curves for three of the samples studied (one at each nominal strain rate) are shown in Figure S2. For these, the hardening coefficient corresponds to the average slope of each of the curves. It is clear that as the rate becomes smaller, the hardening coefficient presents an oscillatory behavior with no apparent monotonic rate dependence (with about 10% slope fluctuations). These fluctuations could certainly be attributed to the sample-to-sample fluctuations. We shall mention that this fluctuation takes place at a time/strain-scale very large compared to the oscillation scale we

discussed in this paper, and thus is not related to the concrete results we presented in the main text and Figure 1 and 2. Moreover, our main conclusions persist if a slight time dependence is incorporated to the parameter  $k$ , resembling the experiments.

Our microcrystals are large enough ( $\sim 25 \mu\text{m}$ ) that their plastic deformation is representative of a comparable subregion of the bulk (which has size independent characteristics). We believe our observed quasiperiodic oscillations and the competition between glide avalanches and slow relaxation are also happening in bulk plasticity at these deformation rates. We show the full timeseries for the three samples chosen to make Figure 2(a) in Figure S3, together with the actual event timeseries before applying our smoothening procedure. Using the smoothened timeseries as a guide to the eye, one may observe that these oscillations of the smoothened timeseries are related to bursts of activity taking place at quasi-periodic intervals. In comparison to the theoretical plot of Figure 2(b) one may also notice that the experimental behavior has additional complexity. Beyond the universal quasi-periodicity, there is a non-trivial event structure during the bursts of activity, with some “shock-aftershock” behavior seen: However, we have not been able to identify a detectable event asymmetry by explicitly calculating the average skewness of the burst activity in a quasiperiod. It is worth noting that the asymmetry in the model of Eq. 1 vanishes as  $k$  is increasing. Intuitively, this behavior can be understood by considering the variance of the  $\rho$  fluctuations in Eq. 4: When  $\rho_0$  is very close to the parent critical point (equivalently  $k \rightarrow 0$ ), an increasing sequence of “shocks” clearly dominates the system behavior.

### **(b) Mutual consistency of the models in Eqs. 1, 4 and verification of the minimal picture**

One may argue that the association of the models of Eq. 4 and Eq. 1 is less than obvious and requires concrete justification. Here, we provide robust numerical evidence that our inter-

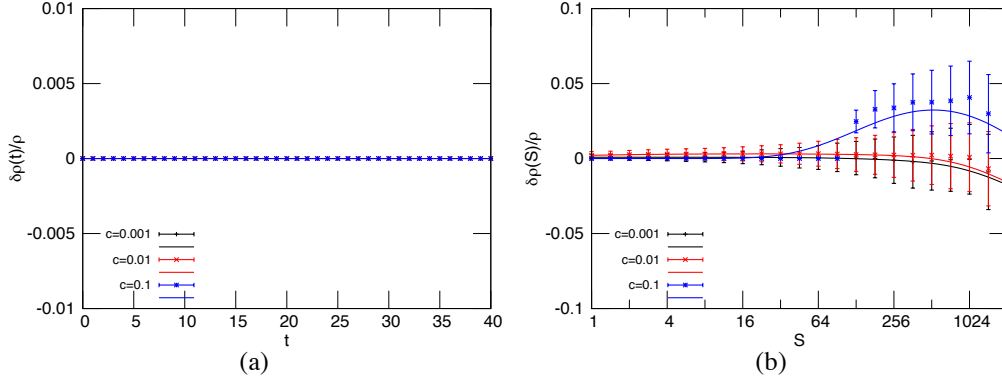


**Figure S4 – The effect of  $c$  on  $\rho$  in the simulations of Eq. 1.** It would be a naive expectation that the increase of the driving rate  $c$  is similar to increasing  $R$ . For  $R = 0$ , but for a finite  $c$ , it is clear that (a) there is no effect of  $c$  in-between the avalanche events and, (b) the difference  $\Delta\rho/\rho$  for the change of  $\rho$  just after an event shows a dependence on  $c$ , but it is on the opposite direction: namely, increasing  $c$  leads to an increase of  $\rho$  after an avalanche before it starts decreasing for very large events. This is a result of the fact that finite  $c$  leads to overlapping avalanches, creating positive correlation among events. Note that the error bars display the *saturated* sample variation, while the lines are Bézier interpolants, weighed by the error bars. A large error bar is a signature that there is a non-trivial intrinsic saturated distribution of  $\Delta\rho$ , as one would expect. Linear binning is used.

pretation of the phenomenon described by Eq. 1 is represented in terms of Eq. 4. Our results are for simulations of Eq. 1 using the parameters mentioned in (A) but also with a simplified infinite-range kernel ( $K(\mathbf{r} - \mathbf{r}') = \text{const.}$ ), which is the *mean-field version* of Eq. 1. The actual kernel used in Eq. 1 shows similar qualitatively results, but we choose to not discuss them here since the numerical correspondence between Eqs. 1 and 4 is qualitative, but not as quantitative and transparent (for the system sizes used). We believe that the correspondence between Eqs. 1 and 4 becomes *exact* only in the infinite-range case but the qualitative picture shall be right for any kernel, even the short-range ones. Since the kernel used in Eq. 1 relevant for plasticity is in the mean-field universality class (27), we believe that the correspondence of Eqs. 1 and 4 is exact in the infinite-system size and quasistatic ( $c \rightarrow 0$ ) limits. Also, we focus on a small  $L = 32$  system (except otherwise mentioned), since the effects we describe in this section con-

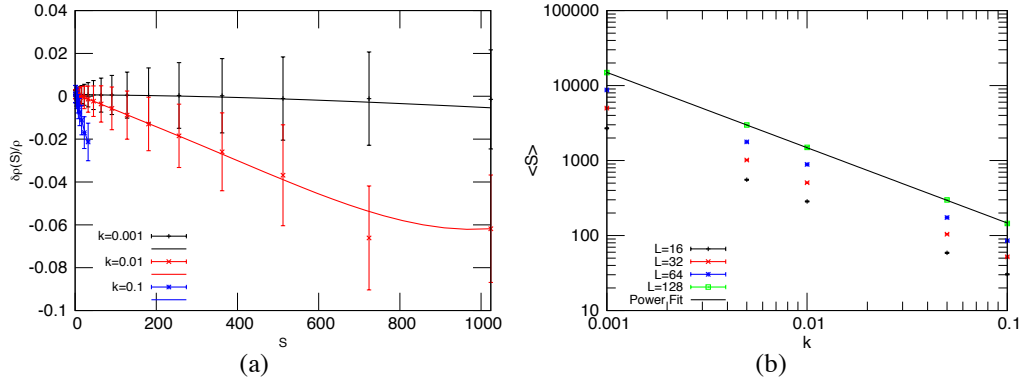


**Figure S5 – The effect of  $k$  on  $\rho$  and reasoning behind the effective model.** (a) A clear linear dependence of  $\Delta\rho/\rho$  on  $k$  is observed in the simulations of Eq. 1. Larger  $k$  denotes a sharper decrease of  $\Delta\rho/\rho$  just after an event, suggesting that  $\rho_{t+1} = \rho_t - A k S_t$ , where  $A$  is a model dependent constant. (b) Moreover, in this model, one easily observes that the average event size scales with  $k$  in a simple manner  $\langle S \rangle \sim 1/k$  (see also (24)), and holds for all system sizes. In this way, we conclude that  $\rho_{t+1} = \rho_t - A \frac{S_t}{\langle S \rangle}$ .

verge for very small system sizes. Note that we do not have, in this paper, any analytical means of “proving” this correspondence, even though we believe it is a tractable but tedious possibility.

In order to compare the structure of Eq. 4 with Eq. 1, we calculate numerically the susceptibility to jumping at every time-step, without counting the steps inside an avalanche. This is done by creating a sorted list of the system’s local stresses  $\sigma$ , subtracting the quenched thresholds  $\sigma_f$  and, by estimating the numerical derivative at the maximum end of this list by averaging it over a small window. Figure S4 shows, as a consistency check, that an increase of the driving rate  $c$  (for  $R = 0$  (*i.e.* zero diffusion) and small  $k$ ) does not affect  $\rho$  in a visible manner. Between avalanches  $\rho$  remains constant as expected and, therefore,  $\delta\rho(t)$  for time- $t$  intervals is zero (Figure S4(a)). Also, after an avalanche, (again for  $R=0$  and small  $k$ ) the change in  $\rho$  is negligible for small event sizes  $S$  but, becomes significant for events that are close to the system size; however, it is not consistently decreasing in a monotonic way. Rather, it increases

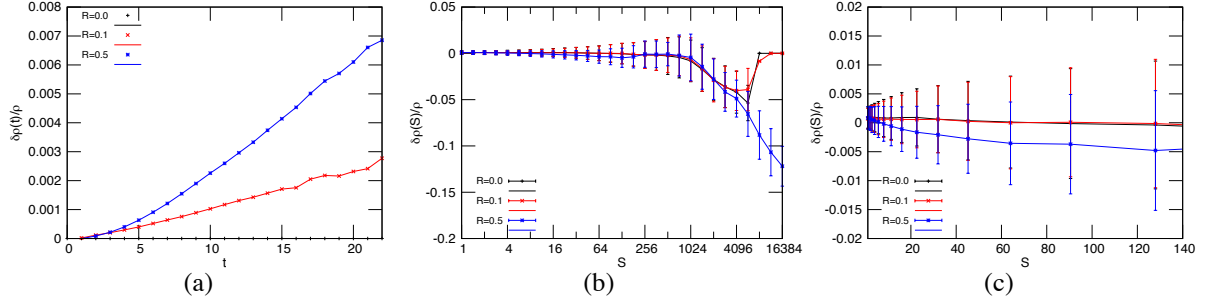


**Figure S6 – The effect of  $R$  in the simulations and motivation behind the effective modeling.** (a) In between events,  $\rho$  increases monotonically with a slope that becomes larger with  $R$ . This behavior suggests that  $\rho_{t+1} = \rho_t + c_d$  where  $c_d \sim R$ . (b), (c) After an event,  $\rho$  monotonically decreases in a way that is proportional to  $R$  in both small (c) and large (b) event sizes, but with different proportionality coefficients. In the effective model we degenerate this difference by considering  $\rho_{t+1} = \rho_t - c_d S_t / \bar{S}$ , where here  $\bar{S}$  serves as a constant. Overall, our observations of Fig. 5, 6 and this one leads to our conclusion that a minimal model is  $\rho_{t+1} = \rho_t + c_d(1 - S/\bar{S})$  where  $c_d \sim R$  and  $\bar{S}$  is the fixed point value for the average size at long timescales.

for intermediate sizes while it decreases for larger ones; a behavior which becomes more evident as the rate becomes larger (for example notice  $c = 0.1$  in Figure S4(b)). The effect of the other free parameter of Eq. 1, the hardening coefficient  $k$ , is more significant (keeping  $R = 0$ ): For large  $k$ , the change of  $\rho$  due to an avalanche is simple  $\delta\rho(S) \sim -kS$ , with small finite system size corrections (cf. Figure S5(a)). Also, notice that the saturated simple standard deviation increases with the size, indicating the existence of a corresponding scaling distribution. Moreover, if we also utilize the fact that  $\langle S \rangle \sim 1/k$  ((24) and Figure S5(b)), we can conclude that  $\delta\rho$  after avalanche events depends crucially on the system's distance from the critical point  $\Delta\rho/\rho \sim S/\bar{S}$  where  $\bar{S} \equiv \langle S \rangle$  for  $R = 0$ .

The situation changes drastically when  $R$  is non-zero: In-between avalanches,  $\rho$  increases in an almost linear manner having a slope that is directly proportional to  $R$ (cf. Figure S6(a)). The result of Figure S6(a) justifies the use of the constant rate  $c_d$  in Eq. 4 and, we identified it as a coarse-grained relaxation (*i.e.* effectively proportional to  $R$ ). Moreover, the presence of a

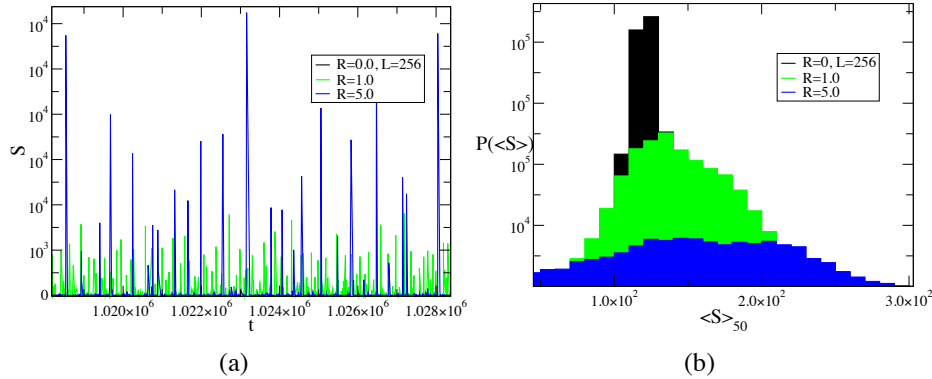


**Figure S7 – A posteriori verification of the minimal picture.** (a) The timeseries of the event sizes is displayed for simulations of different  $R$ s, showing the emerging large events that dominate at large  $R$ . (b) After averaging the timeseries in (a) over a small running time window (50), histograms of the observed average sizes display the expected behavior, as being predicted by our minimal model (and picture) where the behavior of  $\rho$  can account for the relevant effect of  $R$  on the distributions. Note that average size is related to  $\rho$  with a robust relationship, even though  $\langle S \rangle$  is much more intuitive. In the picture, the sharp distribution for  $R = 0$  becomes flatter as  $R$  increases.

finite  $R$  does not significantly alter the response of  $\rho$  to avalanche events for fixed  $k$  (cf. Figure S6(b), (c)), and it ultimately provides a confirmation of the use of Eq. 4 as our minimal model. We note that the construction of Eq. 4 includes an assertion that we neglect all other effects the relaxation might have on the internal structure of the avalanches. It is clear that this is an approximation that might be worrisome in cases where the stress relaxation takes special forms and, if it has symmetries that are not included in the interaction kernel that is activated during avalanches.

Finally, we shall mention that our construction is also verified by the study of the histograms of  $\rho$  and  $\langle S \rangle$  (cf. Figure S7) as  $R$  is increased. Even though the structure of the whole timeseries is altered in a rather complicated manner as  $R$  increases (Figure S7(a)), the expected behavior is clearly present: the observed  $\langle S \rangle \sim \rho^{-\theta}$  (where  $\theta = 1/2$  at mean-field) is spread over a large range, losing its well peaked structure.

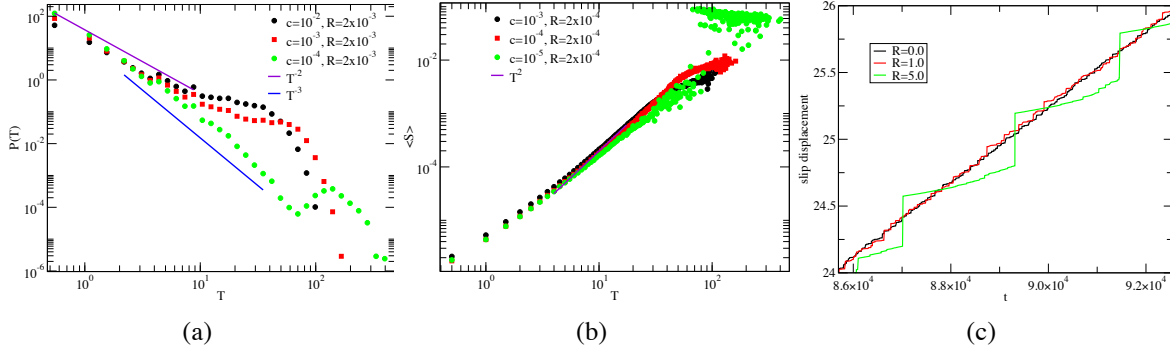


**Figure S8 – Observables in the simulations and consistency.** (a) The duration distributions are shown for the simulations used for Fig. 1(a) and (b), showing that durations display a strong rate dependence, as in the experiments (Fig. 4). (b) The average size vs. duration plot, however, does not display an observable dependence on the rate (also as in the experiments (Fig. 4)), apart from the emerging large event flat profile at very large sizes. The flat profile is a signature of the renewing events that saturate the cutoff behavior of the size distributions (bump) which are absent in the thermodynamic limit. This is just a finite-size effect. In terms of a theoretical interpretation, the absence of such a dependence is supportive of the idea that the effect does not change the  $\sigma\nu z$  exponent of the depinning universality class, a vital signature of distribution integration. (c) In the simulations, the increase of the rate  $c$  (at fixed  $R$ ) or the increase of  $R$  (at fixed  $c$ ), show very similar behavior. The most characteristic feature of it though, is a stick-slip emergence in the displacement vs. time behavior that is displayed. As  $R$  increases, there is an emerging stick-slip and quasi-periodic behavior.

**(c) Analytical properties of Eq. 4 and derivation of the crossover line  $c_d \sim a/\bar{S}$ .**

The probability distribution for Eq. 4 has the peculiar feature that it is divergent on short scales, i.e. it is ultraviolet divergent. If we take

$$P(S) = 1/\mathcal{N} S^{-3/2} e^{-S/S_0} \quad (1)$$

where  $S_0 = 1/(1 - \rho)$  from the main text and  $\mathcal{N}$  a normalization constant, then

$$\mathcal{N} = \int_a^\infty P(S) dS = 2/\sqrt{a} - 2\sqrt{\pi/S_0} + 2\sqrt{a}/S_0 + O(1/S_0^{3/2}) \quad (2)$$

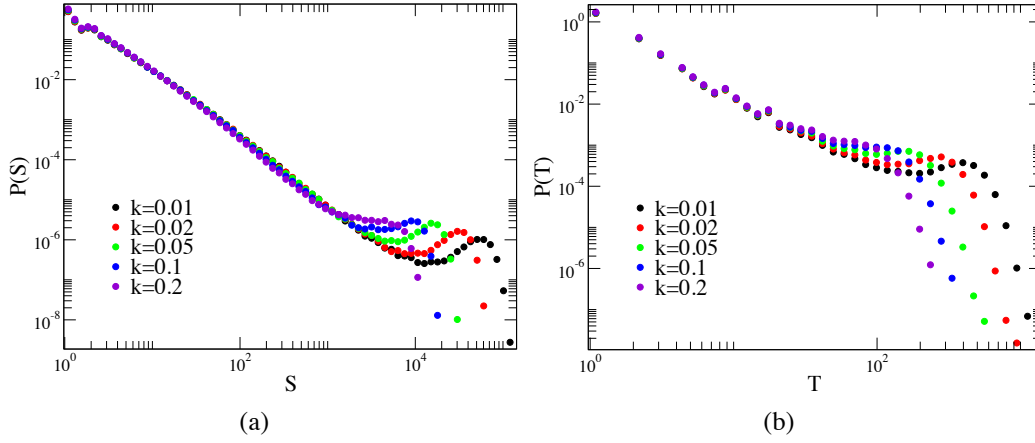


**Figure S9 – Probability distributions as the hardening coefficient increases.** Clearly, the exponent of the critical behavior remains unmodified as the hardening coefficient increases and the cutoff moves to smaller sizes. The data are collapsed with  $\tilde{S} = Sk^{-1.5}$ , apart from the cutoff bump which fades away, consistent with the experiment and our intuitive effective model (Eq. 3), where the bump is not visible. The effective model agrees with this picture, since increasing  $k$  signifies the effective decrease of  $\tilde{S}$  and therefore the large increase of the fluctuations in  $\rho$ . However, in this case, the approach to  $\rho = 1$  becomes improbable.

Then, the average avalanche size comes out to be,

$$\langle S \rangle = \int_a^\infty SP(S)dS = (a\sqrt{\pi}/2)\sqrt{S_0/a} + a(\pi/2 - 1) + a/2(\pi^{3/2} - 3\sqrt{\pi})\sqrt{a/S_0} + O(1/S_0) \quad (3)$$

and in the limit where  $S_0 \rightarrow \infty$  (close to the critical point) we keep the leading term,

$$\langle S \rangle = \frac{a\sqrt{\pi}}{2} \sqrt{\frac{S_0}{a}} \quad (4)$$

The fact that  $\langle S \rangle$  does not scale with  $S_0$  but with its square root, is in the core of the peculiar properties of such special power-law distributions: Generally, let our power law be  $\tau$  (it is  $3/2$  in the case we considered), and let us approximate an exponential cutoff at  $S_0$  as a sharp cutoff.

Then  $\langle S \rangle$  is a ratio of two integrals of power laws, and gives

$$\langle S \rangle = \frac{(2 - \tau)(S_0^{2-\tau} - a^{2-\tau})}{(1 - \tau)(S_0^{1-\tau} - a^{1-\tau})} \quad (5)$$

If  $\tau < 1$ , then we can take  $a \rightarrow 0$  and  $\bar{S} \sim S_0$ . If  $\tau > 2$ , then we can take  $S_0 \rightarrow \infty$  and  $\bar{S} \sim a$ . But if  $1 < \tau < 2$ , we can only take  $a \rightarrow 0$  in the numerator and  $S_0 \rightarrow \infty$  in the denominator, and get

$$\bar{S} \simeq (\tau - 1)\Gamma(2 - \tau)a^{\tau-1}S_0^{2-\tau} \quad (6)$$

which agrees with our previous answer if  $\tau = 3/2$ .

From Eq. 4, the long-time behavior satisfies the fixed point solution  $\bar{S} = \langle S \rangle$  giving that  $\rho$  will fluctuate around the value that satisfies,

$$S_0 = \frac{4a}{\pi}(\bar{S}/a)^2 \quad (7)$$

Since we are focused on the calculation of the crossover line, it is clear that it will take place when large negative jumps of  $\rho$  are proliferating. That requires  $S$  being large enough that  $S/\bar{S} \sim 1/c_d$  leading to  $\Delta\rho_n \sim -1$ . As mentioned in the main text, this is roughly equivalent to saying that  $S_0/\bar{S} \sim 1/c_d$ . In more detail,

$$\begin{aligned} P_{\text{large}}(S_m) &= \int_{S_m}^{\infty} P(S)dS \\ &= \frac{S_0}{2a} \frac{\frac{2e^{-S_m/S_0}}{\sqrt{S_m/a}} - \frac{2\sqrt{\pi}\text{Erfc}(S_m/\sqrt{S_0S_m})}{\sqrt{S_0/a}}}{1 - \sqrt{\pi}\sqrt{S_0/a} + S_0/a} \end{aligned} \quad (8)$$

which in the limit where  $S_m \rightarrow \infty$  (equivalent to saying that  $1/c_d, S_0 \rightarrow \infty$ ),

$$P_{\text{large}} = \frac{\frac{(S_0/a)^2}{(S_m/a)^{3/2}}}{1 - \sqrt{\pi}\sqrt{S_0/a} + S_0/a} e^{-S_m/S_0} \quad (9)$$

Then, for having  $\Delta\rho_n = -1$ , the number of steps to wait is,

$$\begin{aligned} T_w &= 1/P_{\text{large}}(\bar{S}/c_d) \\ &= \frac{\pi (\pi + 4(\bar{S}/a)^2 - 2\pi(\bar{S}/a))}{8 \left(\frac{c_d}{\bar{S}/a}\right)^{3/2} (\bar{S}/a)^4} e^{\frac{\pi}{4} \frac{1}{c_d \bar{S}/a}} \\ &\cong \frac{1}{c_d} \frac{\pi}{2} \frac{e^{\frac{\pi}{4} \frac{1}{c_d \bar{S}/a}}}{\sqrt{c_d \bar{S}/a}} \end{aligned} \quad (10)$$

After each such big avalanche,  $\rho$  spends a long time ascending towards the critical point, which corresponds to an integration procedure which alters the critical exponents. The number of time steps of integration (assuming the large jump gives  $\rho = 0$  just after the jump) is,

$$T_a = \frac{1}{c_d} \quad (11)$$

neglecting all corrections that involve  $S/\bar{S}$ . The crossover line takes place when  $T_w/T_a \simeq 1$ , which ultimately gives us the solution, in the limit  $\bar{S} \rightarrow \infty$  that the crossover line takes place when,

$$c_d \simeq \frac{3.751}{\bar{S}/a} \quad (12)$$

The simulations which led to Fig. 3 of the main text are consistent with  $c_d \simeq 8/(\bar{S}/a)$  as one can easily check. The discrepancy of the constant is due to deficiencies of the theoretical calculation, since it does not include jumps smaller than 1 which are abundant near the crossover line and it does not take into account the boundary condition at  $\rho = 1$  (in the simulations,  $\rho$  is reset to a random position after such a jump contributing also to the integration). However, the trend is captured correctly ( $\sim 1/(\bar{S}/a)$ ). The fact that  $c_d$  is dimensionless is consistent with all our previous findings that point to that we are describing a true, novel critical behavior (quasiperiodic oscillating behavior) which is system-size independent (but certainly, UV-dependent). Since it is a true, novel critical behavior, it is rather possible that the two regimes are separated by another phase transition (instead of a crossover), a possibility that requires further investigation since it is rather complicated to find evidence for.

#### **(d) Details and conclusions of the simulations of Eq. 1**

Here, we provide a more complete picture of the simulations of Eq. 1 that we described in the main text. While there are several aspects that will be carefully studied in subsequent publications, there are some main observations and conclusions we can draw herein. In Figure S8,

we show the behavior of durations for the same simulations discussed in the main text (Figure 2). First, we note that durations correspond to the times taken for jumps in the displacement (cf. Figure S8(a)). As we described in the caption of Figure 2, in order to compare with experiments we needed to assume that this duration is finite and corresponds to the number of cellular automata steps inside the avalanche. This picture is *a posteriori* consistent, since the experimentally relevant time step is significantly smaller than the timestep of the external stress increase. However, this is just a working assumption about the dynamics of the avalanches and the situation could certainly be more complex. Overall, the durations display distributions that are consistent with the experiments and also consistent with our minimal picture. As seen in Figure S8(b), the durations have a scaling distribution and drifting exponent  $\alpha$  from  $2.0 \pm 0.1$  to  $3.0 \pm 0.2$ , with changing strain rate. This finding is consistent with Figure S1. The behavior of  $\langle S \rangle$  also displays a power-law with respect to the avalanche duration ( $\langle S \rangle \sim T^{1/\sigma\nu z}$ ) which stays visibly invariant as  $c$  decreases (cf. Figure S8(c)). There is a plateau for large durations, we have checked that this feature disappears as the system size increases.

In Figure S9, we show the behavior of the size distributions (for fixed relaxation and driving rates  $R = 2$ ,  $c = 0.000125$ ) as  $k$  increases for  $L = 128$ . For  $k = 0.01$  the system already displays strong quasi-periodic behavior that we described. A fixed system size controls the avalanche size cutoff scale  $S_0$  according to the formula  $S_0 \simeq 2L^{0.85}/k$ . From Figure S9, it is straightforward to observe that the critical exponents of sizes (Figure S9(a)) and durations (Figure S9(b)) are invariant to the change in the cutoff scale and, therefore, we conclude that the distance from the parent critical point (controlled by  $k$ ) does not alter the integration effect (see Eq. 4) on the critical distributions. This result, together with the inset of Figure 3(a), signifies that the integration effect we report *does not depend* on the distance of the system from the critical point before  $R$  is turned on. However, it is also easy to notice that the distance from the critical point strongly affects the functional form of the distribution near the cutoff. When

the system for  $R = 0$  is near to the parent critical point (small  $k$ ) the size and duration distributions display a characteristic “bump” near the cutoff. This bump is the finite-size signature of avalanches that percolate, which equivalently corresponds to  $\rho$  becoming equal to 1 before these avalanches take place. However, as expected this bump *vanishes* when  $k$  increases, but with no visible change in the critical exponents. In a qualitatively similar manner, the bump vanishes when the system size increases (Figure S10(b)) or when  $R$  decreases (Figure S10(a)). Overall, this evidence signifies that the phenomenon we describe corresponds to *true* critical behavior as relaxation processes are present in the system, and not a special finite size effect.

Finally, we present some relevant conclusions about the simulations that we shall describe in detail in a future publication: First, the quasi-periodicity and associated integration (see Eq. 4 and discussion therein) is present for all interaction kernels we checked in two dimensions:  $K(\mathbf{k}) = |\mathbf{k}|, \mathbf{k}^2$ , or const. all display the reported phenomenon as  $R$  increases. The kernel  $|\mathbf{k}|$  was studied in (20) for a single slip plane of mixed dislocations, and  $\mathbf{k}^2$  corresponds to a local kernel which leads to avalanche critical behavior in the short-range interface depinning universality class (7). Second, the quasi-periodicity and associated integration appears for several functional forms for the stress relaxation term of Eq. 1; We have explicitly checked a) local  $\phi$  diffusion ( $\sim \nabla^2 \phi$ ), b) non-local diffusion ( $\sim (\langle \phi \rangle - \phi)$ ), c) local stress diffusion (acting between  $\phi$  slips,  $\phi$  evolves in a way that  $d\sigma/dt \sim \nabla^2 \sigma$  is satisfied). We believe that the case studied in (9) strongly resembles the much simpler model of  $K(\mathbf{k}) = |\mathbf{k}|$  and the (c) type of relaxation. All of these models belong to the same class displaying the general phenomenon described in this paper.

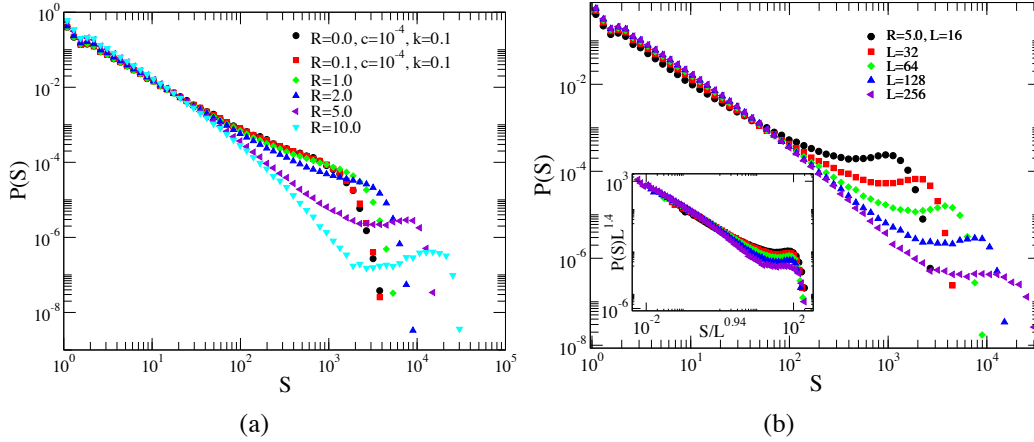


**Figure S10 – Probability distributions as  $R$  increases and stability with system size.** (a) As  $R$  increases, the model of Eq. 1 displays quasiperiodic oscillations and the exponent  $\tau$  of the size distribution drifts to 2.5 from the original 1.5. Notice that the distribution displays a “bump” at the cutoff, which grows as  $R$  increases. This bump corresponds to large events close to the critical point, which cause large changes of the jumping susceptibility. However, the bump is a finite-size effect, since it goes away when the system size increases or when  $k$  decreases. (b) For fixed  $R$ , the system size dependence is studied for  $P(S)$ , showing a consistent scaling collapse with  $\tilde{S} \sim SL^{-0.94}$  (inset). We shall note that for  $R = 0$ , the size distribution does *not* scale with the system size (the hardening coefficient has been chosen accordingly to scale with the system size in order to achieve this), in order to isolate the system size dependence related to  $R$ . The only non-collapsing part is the “bump” region, where the bump consistently disappears in the large system-size limit, signifying that the system *never* crosses the parent critical point to the infinite-avalanche phase (i.e. large events are scale invariant, part of the scaling behavior and do not scale with the system size). The details of this behavior will be discussed elsewhere.